MOTOR CURRENT SIGNATURE ANALYSIS TO DETECT FAULTS IN INDUCTION MOTOR DRIVES—FUNDAMENTALS, DATA INTERPRETATION, AND INDUSTRIAL CASE HISTORIES

by

William T. Thomson

Director and Consultant

EM Diagnostics Ltd.

Alford, Aberdeenshire, Scotland

and

Ronald J. Gilmore

Discipline Technical Authority (Electrical Engineering)

AMEC Upstream Oil & Gas

Nigg, Aberdeen, Scotland

William T. (Bill) Thomson has been Director and Consultant with EM Diagnostics Ltd., in Alford, Aberdeenshire, Scotland, since August 2001. He has 42 years' experience covering the installation, maintenance, design, performance, and condition monitoring of electrical drives. Professor Thomson has worked as electrician, R&D engineer, academic, and consultant. In 1990, he was appointed Professor at Robert Gordon University in Aberdeen, Scotland, for his research and development work on condition monitoring for electrical drives. He was awarded a First Class Technological Certificate in Electrical Installation work from The City & Guilds London Institute (1966), and a Higher National Certificate in Electrical Engineering (1970)

Professor Thomson has a BSc (Hons, Electrical Engineering, 1973) and an MSc (1977) from the University of Strathclyde, Scotland. He is a SMIEEE and FIEE, a CEng in the UK, a visiting Professor in Electrical Engineering at the University of Abertay, Scotland, and has published over 70 papers.

Ronald J. (Ron) Gilmore is Discipline Technical Authority (Electrical Engineering) with AMEC Upstream Oil & Gas, in Nigg, Aberdeen, Scotland. He has worked in the electrical industry for 37 years covering installation, maintenance, and design in the marine, high voltage, and oil and gas sectors. Mr. Gilmore began his career as an electrician in the marine industry and presently holds the position of Discipline Technical Authority for multiple assets including offshore oil and gas production platforms and onshore gas processing plants. His responsibilities include the safe and reliable operation of 113 MW of generation capacity and associated distribution systems up to a voltage level of 11 kV. He is also responsible for the maintenance and operation of electric drives up to a rating of 14 MW.

Mr. Gilmore was awarded a Higher National Certificate (Electrical Engineering, 1975), and is an Associate Member of the Institute of Electrical Engineers in the UK.

ABSTRACT

Induction motor drives are the most widely used electrical drive system and typically consume 40 to 50 percent of an industrialized nation's total generating capacity. In the USA the total generating capacity is approximately 800,000 MW; consequently induction motor drives are major assets in the process and energy industries. Motor current signature analysis (MCSA) is a condition monitoring technique that is now widely used to diagnose problems such as broken rotor bars, abnormal levels of airgap eccentricity, shorted turns in low voltage stator windings, and certain mechanical problems. This tutorial sets out to present the fundamentals on MCSA plus data interpretation and the presentation of industrial case histories.

INTRODUCTION

The operators of induction motor drives are under continual pressure to reduce maintenance costs and prevent unscheduled downtimes that result in lost production and financial income. Many operators now use online condition-based maintenance strategies in parallel with conventional planned maintenance schemes. However, it is still the operator who has to make the final decision on whether to remove a motor from service or let it run based on information from condition monitoring systems. This tutorial paper is presented in the recommended style of a tutorial and, to quote the guidelines, the purpose of a tutorial is to teach, not just review. At the discussion of a paper presented by Thomson and Orpin (2002) at the Thirty-First Turbomachinery Symposium, several key questions were asked by the audience, and this tutorial also addresses these points. The question by mechanical engineers/vibration diagnosticians was "but surely the problem of broken rotor bars can be detected via vibration monitoring, would the authors like to comment?"

A crucial point about motor current signature analysis (MCSA) is that it is sensing an electrical signal that contains current components that are a direct by-product of unique rotating flux components caused by faults such as broken rotor bars, airgap eccentricity, and shorted turns in low voltage stator windings, etc. MCSA can detect these problems at an early stage and thus avoid secondary damage and complete failure of the motor, as reported by Hargis, et al. (1982), Thomson (1984), Thomson and Rankin (1987), and Kliman and Stein (1990). It is true that broken rotor bars will result in a change to the vibration spectrum, but vibration is traditionally sensed at the bearings. And for each motor there is a different mechanical stiffness between the electromagnetic forces caused by broken bars and the position where the vibration is

sensed. This adds an additional complexity when attempts are made to quantify the severity of the problem via vibration analysis. Electromagnetic forces are proportional to the flux density squared waveform (Alger, 1965; and Yang, 1981) in an induction motor. Hence, the vibration from unique electromagnetic forces from broken bars, etc., is a second order effect compared to current components directly induced from the specific rotating flux waves. In many cases the fault severity (e.g., number of broken rotor bars) has to be serious before it can be detected by vibration analysis, and even then the prediction of fault severity is another order of magnitude more difficult.

This is not the case with MCSA as has been proven via numerous industrial case histories. With respect to detecting airgap eccentricity problems, a similar reasoning applies as explained above and as reported by Cameron, et al. (1986), Tavner and Penman, (1987), and as demonstrated via industrial case histories by Thomson and Barbour, (1998) and Thomson, et al. (1999). With respect to detecting shorted turns in low voltage stator windings then Thomson (2001) has shown that MCSA can detect the fault before a phase-to-phase or phase-to-earth failure. It is therefore possible with a low voltage (LV) stator winding to have some lead time between shorted turns developing and actual failure. In comparison to a high voltage (HV, e.g., 4160 V and above) induction motor, the time to failure with an interfault will be very short indeed.

TUTORIAL OBJECTIVES

Motor current signature analysis can diagnose problems such as broken rotor bars, abnormal airgap eccentricity, shorted turns in low voltage stator windings, and certain mechanical problems/drive train characteristics as reported in a major review paper by Thomson (1999). The primary objectives of this tutorial are to provide users with the fundamentals of MCSA and to illustrate its application via industrial case histories. Note that faults and their causes will be embedded within the tutorial, and the reader is referred to the references for more details on faults and causes in three-phase induction motors. This tutorial paper includes:

- Definition and explanation of motor current signature analysis.
- Reliable current sensing, spectrum analysis specifications, and MCSA instrumentation.
- Fault mechanisms and interpretation of current signatures.
- Sample of MCSA case histories—note that additional case histories will be presented at the tutorial presentation.

MOTOR CURRENT SIGNATURE ANALYSIS

Motor current signature analysis is the online analysis of current to detect faults in a three-phase induction motor drive while it is still operational and in service as shown in Figure 1. A basic MCSA instrumentation system will consist of the following:

- A current transformer (CT) to sense the signal.
- A resistive shunt across the output of the CT—note that CTs are available with internal shunts.
- An MCSA instrument (or spectrum analyzer) to produce the current spectrum or signature.

An idealized current spectrum is shown in Figure 2 that, in this illustration, represents the twice slip frequency sidebands due to broken rotor bars. Note that a decibel (dB) versus frequency spectrum (referred to as linear root-mean-square (rms)) is used to give a wide dynamic range and to detect the unique current signature patterns that are characteristic of different faults. Depending on the actual onsite installation, the CT can be of two types, namely a clip-on CT around one of the phases of the supply cable as shown in Figure 3, or around the secondary side of an existing instrumentation CT in the instrumentation panel as shown in Figure 4. Note that only one CT is required for MCSA, and it can be in any one of the three phases. The fundamental reason for this is that the rotating flux waves produced by the different faults cut all three stator phase windings, and corresponding currents are induced in each of the three phases.

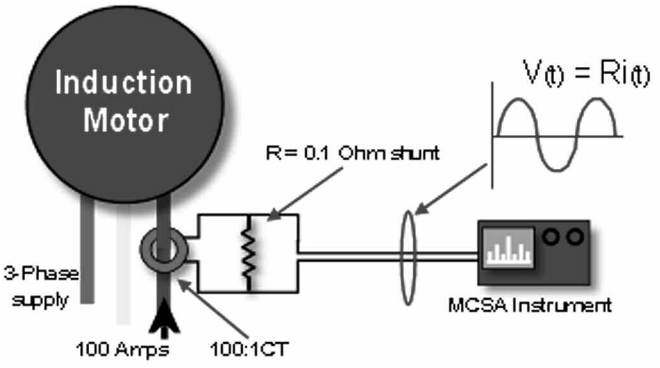

Figure 1. Basic MCSA Instrumentation System.

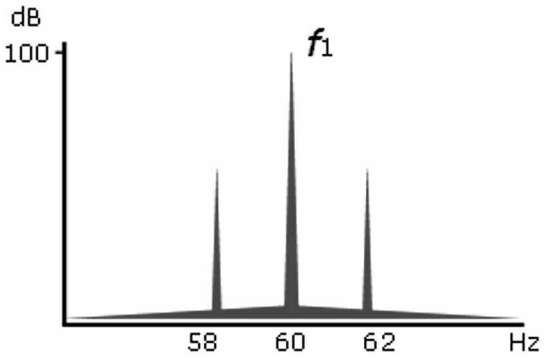

Figure 2. Illustration of Current Spectrum.

Figure 3. Clip-on CT Around Supply Cable.

Typical CT Requirements

Since a question on CT specifications was raised at the 2002 Symposium, here is a typical specification for a commercially available CT that has been successfully used for MCSA:

- Input current range: 1 A to 600 A
- Accuracy: ±2 percent of reading 50 Hz to 1 kHz; ±3 percent of reading, 30 Hz to 50 Hz and 1 kHz to 10 kHz
- Working volts: 750 V, AC rms maximum. Maximum conductor size: 2 inches (50.8 mm)

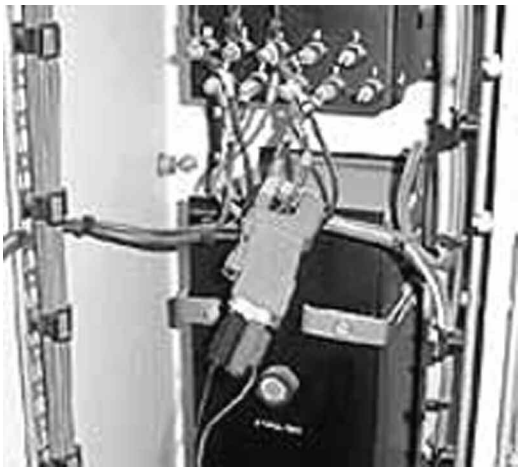

Figure 4. Small Clip-on CT Around the Secondary of Existing Instrumentation CT.

- Safety: Protection class II as defined in IEC 348 and NSI C39.5
- Resistive shunts: 1 A to 10 A (10 ohms), 10 A to 200 A (1 ohm), 200 A to 600 A (0.1 ohm)

The high frequency response is required to cover the frequency range of components that can be induced due to different fault mechanisms found in a wide range of designs of three-phase induction motors and also to cater for inverter fed (variable speed) induction motor drives. If necessary, more technical details on in situ instrumentation CTs and clip-on CTs of the type shown in Figures 3 and 4 will be provided at the actual tutorial presentation.

Typical MCSA Signal Processing Specifications

Detection of Broken Rotor Bars

Definition and explanation of slip of an induction motor are presented in APPENDIX A. To cope with low full-load slips such as 0.55 percent or 0.0055 per unit (lowest that the author has encountered), then the fast Fourier transform (FFT) line resolution should be, for example: 7.8 milliHz/line (12,800 lines in a baseband mode of zero to 100 Hz). With this resolution, the analysis time t = 1/line resolution = 1/0.0078 = 128 sec. If the full-load slip is 1 percent (0.01) or greater, then the line resolution can be 15.6 milliHz/line (analysis time t = 64 sec). It must be remembered that a motor may well be operating at less than full-load. The detection of the twice slip frequency sidebands on no-load is not possible since the current in the rotor bars is negligible. However, the author has found that it is possible to detect broken rotor bars if the load on the motor produces a slip of greater than 35 percent of the full-load slip, but a correction factor has to be applied to estimate the number of broken bars when the motor is operating on a reduced load.

Detection of Abnormal Airgap Eccentricity

A frequency resolution of 100 milliHz/line should be sufficient. Suitable filtering will normally be applied to remove the supply frequency component to identify the current signature pattern that is indicative of airgap eccentricity.

Detection of Shorted Turns in Low Voltage Stator Windings

A frequency resolution of 31.2 milliHz/line should be adequate. The dB dynamic range should be 80 dB or greater for all the above cases.

FAULT MECHANISMS AND MCSA CASE HISTORIES

Figure 5 illustrates the key elements for the successful application of MCSA, these include:

- Fundamental understanding of the design and operation of three-phase induction motors.
- MCSA instrument (or spectrum analyzer) to present the signature patterns.
- Expert knowledge base via expertise within the user's organization and/or external consultants.
- Finally it is the drive operator who has to make the final decision to either immediately remove the motor for repair or let it run and prepare for a planned outage to rectify the problem.

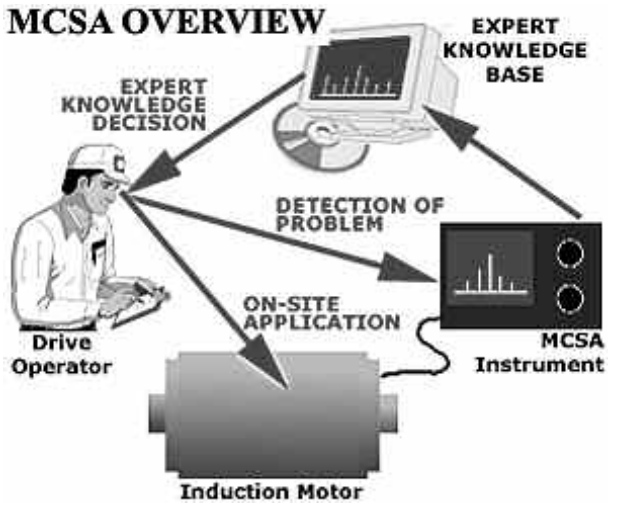

Figure 5. Overall MCSA Strategy.

The specification of the measurement to present the current spectra for different fault mechanisms is a key feature, but this can only be done from an understanding of three-phase induction motors and the signature patterns that are produced by specific faults. Figure 6 is an example of a broken rotor bar problem.

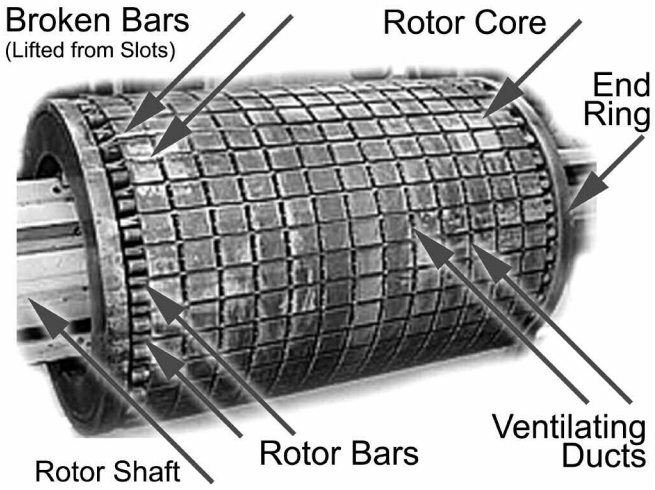

Figure 6. Example of Broken Rotor Bar Problem.

Broken Rotor Bars in Cage Induction Motors

The application of MCSA in industry during the past 10 years has shown that broken rotor bars can be a serious problem with certain induction motors due to arduous duty cycles. Although broken rotor bars do not initially cause an induction motor to fail, there can be serious secondary effects. The fault mechanism can result in broken parts of the bar hitting the end winding or stator core of a high voltage motor at a high velocity. This can cause serious mechanical damage to the insulation and a consequential

winding failure may follow, resulting in a costly repair and lost production. Figure 7 shows a case where a broken rotor bar had lifted in the slot, and the resultant damage to the high voltage stator winding is shown in Figure 8. (Figures 7 and 8 refer to a three-phase, 11 kV, 2900 kW (3887 hp), 179 A, 50 Hz, 2978 rpm, squirrel-cage induction motor (SCIM).)

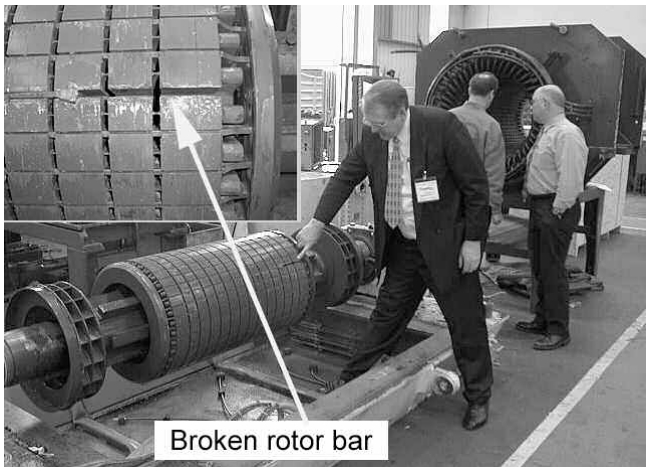

Figure 7. Broken Rotor Bar Lifted out of the Slot.

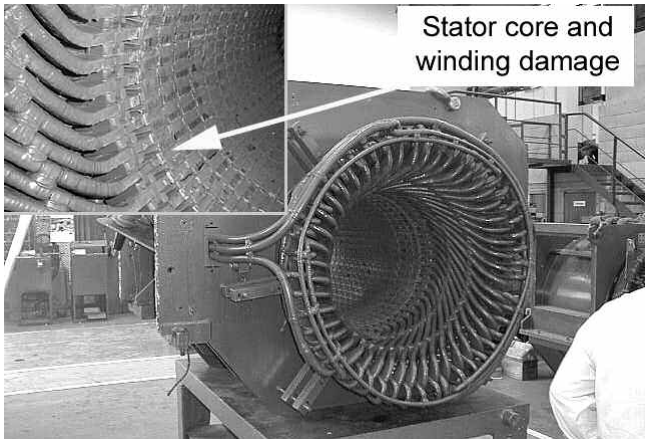

Figure 8. Mechanical Damage to HV Stator Winding.

The repair cost was $160,000 for a replacement rotor and a complete rewind of the stator winding. Fortunately there was a dual drive train to deliver the process on the offshore oil production platform, but this is not always the case since single drive trains are now more common to reduce capital cost, weight, and size of offshore oil production platforms. In hazardous environments, sparking at the fault site during the degradation process can be a potential safety hazard. Operators of large high voltage induction motors cannot take unnecessary risks, hence MCSA is now being extensively used to assess the operational condition of rotor cage windings.

Several excellent papers have been published on rotor bar failures and their causes by Bonnet and Soukup (1992) and Finley and Hodowanec, (2001). Suffice to state that broken rotor bars or end rings can be caused by the following:

- Direct-on-line (DOL) starting duty cycles for which the rotor cage winding was not designed to withstand—this causes high thermal and mechanical stresses.
- Pulsating mechanical loads such as reciprocating compressors or coal crushers (etc.) can subject the rotor cage to high mechanical stresses.
- Imperfections in the manufacturing process of the rotor cage.

Additional examples of broken rotor bar failure are shown in Figures 9 and 10. The rotor in Figure 9 was from a crane motor subjected to DOL starts and had a long run up time (45 sec!). This rotor was not fit for purpose and was not producing sufficient starting torque for the load starting condition. Note the narrow bars and the classic crescent-shape breaks of the actual bars. Figure 10 shows a rotor from a food mixer motor that was being subjected to 24 starts per hour, which again was just too arduous a duty cycle for the rotor design. New designs were implemented and the problems were eliminated.

Figure 9. Crane Motor—Broken Rotor Bars.

Figure 10. Food Mixer Motor—Broken Rotor Bars.

Basic Theory—Qualitative

A full mathematical analysis (with experimental verification) of a three-phase induction motor operating with broken rotor bars was published by Williamson and Smith (1982)—this gives an excellent indepth analysis. A conceptual explanation is now presented to assist the reader in gaining a physical understanding of what happens in an induction motor with broken rotor bars. For completeness, an accompanying mathematical derivation is presented in APPENDIX A.

It is well known that a three-phase symmetrical stator winding fed from a symmetrical supply will produce a resultant forward rotating magnetic field at synchronous speed, and, if exact symmetry exists, there will be no resultant backward rotating field. Any asymmetry of the supply or stator winding impedances will cause a resultant backward rotating field from the stator winding.

Now apply the same rotating magnetic field fundamentals to the rotor winding, the first difference compared to the stator winding is that the frequency of the induced voltage and current in the rotor winding is at slip frequency and not at the supply frequency: s =

per unit slip, f_1 = supply frequency Hz, $f_2 = sf_1$ Hz, f_2 = slip frequency of rotor currents Hz.

The rotor currents in a cage winding produce an effective three-phase magnetic field, which has the same number of poles as the stator field but it is rotating at slip frequency (f_2) with respect to the rotating rotor. When the cage winding is symmetrical, there is only a forward rotating field at slip frequency with respect to the rotor. If rotor asymmetry occurs, then there will be a resultant backward rotating field at slip frequency with respect to the forward rotating rotor. The result of this is that, with respect to the stationary stator winding, this backward rotating field at slip frequency with respect to the rotor induces a voltage and current in the stator winding at (refer to APPENDIX A for the derivation):

$$f_{sb} = f_1(1 - 2s)Hz \quad (1)$$

This is referred to as a twice slip frequency sideband due to broken rotor bars. There is therefore a cyclic variation of current that causes a torque pulsation at twice slip frequency ($2sf_1$) and a corresponding speed oscillation that is also a function of the drive inertia. This speed oscillation can reduce the magnitude (amps) of the $f_1(1-2s)$ sideband, but an upper sideband current component at $f_1(1 + 2s)$ is induced in the stator winding due to the rotor oscillation. This upper sideband is also enhanced by the third time harmonic flux. Broken rotor bars therefore result in current components being induced in the stator winding at frequencies given by:

$$f_{sb} = f_1(1 \pm 2s)Hz \quad (2)$$

This gives $\pm 2sf_1$ sidebands around the supply frequency component f_1. These are the classical twice slip frequency sidebands due to broken rotor bars.

These are sometimes referred to as the pole pass frequencies by condition monitoring practitioners, but this is not really an appropriate terminology and can cause confusion. The publications by electrical machine designers, researchers, and manufacturers always refer to the twice slip frequency sidebands due to broken bars, as can be verified by reading the references in this paper.

Due to the variables that affect the frequency of these sidebands and their magnitude in amps (normally in dB in a MCSA system), the diagnostic strategy has to consider the following:

- Different rotor designs (effect of pole number and number of rotor slots, etc.).
- A wide range of power ratings.
- Different load conditions.
- Mechanical load characteristics.
- Mechanical components in the drive train.

These factors can significantly affect the diagnosis and need to be considered in the development of reliable MCSA instrumentation systems for three-phase induction motors.

Diagnostic Strategy

The primary objective is to carry out a high resolution Fourier analysis of the supply current to the motor to identify the twice slip frequency sidebands. It has to be appreciated that the motor can be operating at different load conditions, hence the slip (s) is a variable and the supply frequency (f_1) is not necessarily exactly the nameplate value or the supply authority's stated value. Variations in these two variables influence the value of the sidebands in Hertz. Since it is only the current that is being analyzed, the MCSA system has to accurately predict the frequency of the sidebands for the particular operational condition of the motor. An MCSA diagnosis has to be able to do this for a wide range of motor designs and ratings, and an estimate of the severity of rotor asymmetry is also required. This has to take into account the operational load condition at the time of the analysis, since with a given number of broken rotor bars the magnitude (dB) of the sidebands is a function of the load. The rotor design has also to be considered. Recommendations to the operator for the next course of action following the identification of broken rotor bars have to take into account factors such as:

- Severity of the fault and rotor design.
- Strategic importance of the drive.
- Operational duty cycle.
- Potential for secondary damage to a high voltage winding and safety issues.

All these requirements clearly need a reliable MCSA instrument, expert interpretation of measured data, expertise in induction motor design and operation, and plant management decisions following the diagnosis of a problem/fault. This involves a combination of advanced technological tools and human expertise.

MCSA Broken Rotor Bar Case Histories

Case History 1—Large Sea Water Injection Pump—Offshore Oil Production Platform

Motor nameplate data: three-phase, SCIM, 6600 V, 3.6 MW/4285 hp, 60 Hz, 376 A, 3580 rpm, star connected. The rotor was copper fabricated, single cage, nose joint design between bars to end ring, 46 rotor bars. The first step is to calculate the full-load slip: $s_{f.l.} = (3600 - 3580)/3600 = 0.0055$. (Refer to APPENDIX A for explanation and definition of slip in an induction motor.) Note that this large motor has a low full-load slip value of 0.0055 or 0.55 percent. Figure 11 is an FFT zoom current spectrum from a routine survey using MCSA. When the motor is operating at full-load current, then the predicted twice slip frequency sidebands for a nameplate frequency of 60 Hz and a full-load speed of 3580 rpm are ±0.66Hz.

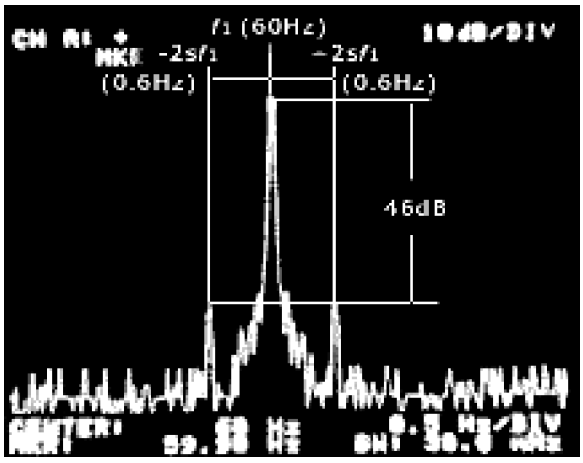

Figure 11. Current Spectrum—Healthy Rotor.

Examination of Figure 11 shows that there are sidebands at ±0.6Hz around f_1 the supply frequency that was 59.9 Hz and not 60 Hz. The measured sidebands therefore correspond to within less than 10 percent of the predicted values using full-load nameplate data since the motor was actually operating at full-load current. In Figure 11 the sidebands are greater than 45 dB down on the supply current, and this corresponds to a healthy working unit for a two-pole motor of this design and rating having 46 rotor bars. Although there are sidebands, it means the rotor is not perfect and there is some rotor asymmetry due to inherent differences in the bar to end ring joints.

At a later date, due to operational problems, this motor was stalled and was then subjected to more than the normal direct-on-line starts.

Due to the incident that occurred, MCSA was applied to assess the condition of the rotor winding. Figure 12 shows the current zoom spectrum and the twice slip frequency sidebands are at ±0.7 Hz. The dB difference between the sideband magnitudes and the supply frequency component is now 26 dB, and this is indicative of a serious broken rotor bar problem. In comparison to Figure 11, the magnitude of the sidebands has increased by 20 dB, which is a factor of 10 times larger in the absolute units of amps.

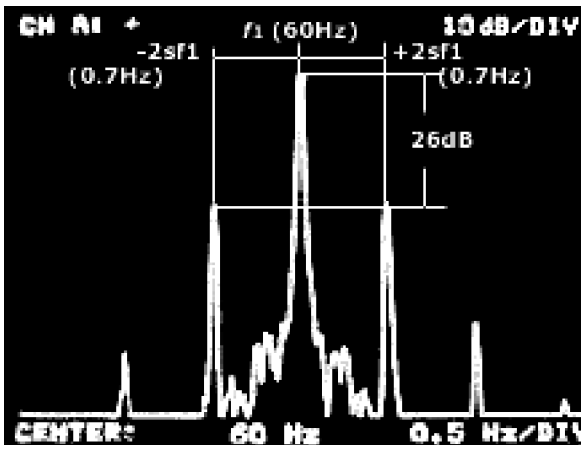

Figure 12. Current Spectrum—Broken Bars.

The recommendation was that the motor should be immediately removed from service since the rotor cage winding was in an extremely unhealthy state. It was a high voltage motor operating on an offshore oil production platform and secondary damage to the motor was a possibility, plus the safety implications had also to be considered. The motor was immediately removed from service, and Figure 13 shows an actual photo of the faulty rotor. As predicted, there were numerous broken rotor bars. There were in fact 20 broken bars.

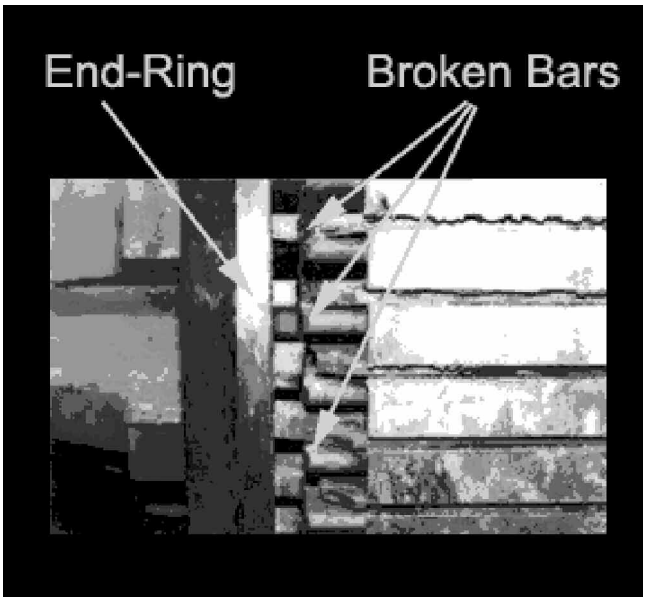

Figure 13. Photo of Unhealthy Rotor Condition—20 Broken Rotor Bars in a Rotor with 46.

Please note that MCSA can be applied at any time and a previous result is not required for comparison. A dB difference of 26 dB from a one-off measurement, as shown in Figure 12, equates to a serious broken rotor bar problem.

Case History 2—Large LP Compressor Motor—Offshore Oil Production Platform

This is a very recent case history, and it is concerned with a strategic low pressure compressor motor drive operating on a North Sea (off the coast of Scotland) oil and gas production platform. Stats are: drive train, LP compressor; motor, three-phase; 11 kV; 1950 kW (2614 hp); 120 A; 50 Hz; 1485 rpm; SCIM; number of rotor bars, R = 60.

There was only one drive train available and downtime results in lost production of seven million standard cubic feet of gas/day ($18,118 lost/day). The gas is derived from processes on the platform such as stripping gas in the deaerator for the sea water injection system. If this LP compressor drive is not operating, then the gas has to be flared off to maintain operation. In line with UK restrictions on gas flare-off rates, the gas flare target on this platform is 0.86 million standard cubic feet of gas per day. If this LP compressor drive is down, the gas flare-off increases to more than seven million standard cubic feet/day. This is over eight times the target figure, requiring consent from the UK Department of Trade and Industry.

If the broken rotor bar fault had gone undetected and resulted in an HV stator winding failure, this would require an in situ rewind on a North Sea offshore oil and gas production platform. The rewind would require three months to complete at a cost of approximately $300,000, and the potential financial loss from lost gas production would be $1.63 million, giving a total loss of nearly $2 million.

It will now be shown how MCSA avoided the type of problems that had previously occurred and are shown in Figures 7 and 8. Failure of this crucial motor was prevented.

MCSA Procedures and Interpretation for this LP Compressor Drive

- *Step one*—Calculate the full-load slip $s_{f.l.} = (1500 - 1485)/1500 = 0.01$

- *Step two*—Calculate the twice slip frequency sidebands due to broken rotor bars at full load = $\pm 2 \times 0.01 \times 50 = \pm 1$ Hz. That is, sidebands due to broken rotor bars at ±1 Hz around the supply frequency component at 50 Hz.

- *Step three*—Prior to the actual MCSA measurement, the actual reading on the in situ ammeter was recorded: I = 104 A (±2 percent). It is recommended practice to record this reading as part of the MCSA procedure. It was noted that there was a small oscillation about a mean position on the analogue ammeter reading. Please note that this is an observation and cannot be used to reliably detect broken rotor bars or to quantify the severity of a fault. Similar effects can occur due to normal oscillating loads/fluctuating loads, effects of low speed gearboxes, and recycling effects in compressors, etc. The whole objective is to gather all the evidence when crucial decisions have to be made about a drive's operational condition. Note that routine bearing vibration measurements by an offshore contractor indicated that no changes had occurred.

- *Step four*—The full-load rated current is 120 A and the motor was taking 104 A. This means the motor will be running at a higher speed than the full-load value of 1485 rpm and, consequently, the slip will be lower, hence the twice slip frequency sidebands will be less than ±1 Hz.

- *Step five*—Select a frequency resolution to ensure an accurate measurement to detect any sidebands from broken rotor bars at the reduced operating load. The analyzer had a fixed number of lines (400) for the selected frequency band. A zoom analysis band of 6 Hz was selected around the supply component (nominally 50 Hz). This gives 15 milliHz/line and an analysis time = 67 sec.

Record a current spectrum dB (V rms) versus frequency (linear spectrum) according to the frequency resolution specification

given in step five. Note: use a dB (V rms) instead of a power spectrum since the supply component of current can then be calculated to validate the current signal being analyzed. Figure 14 shows the current spectrum.

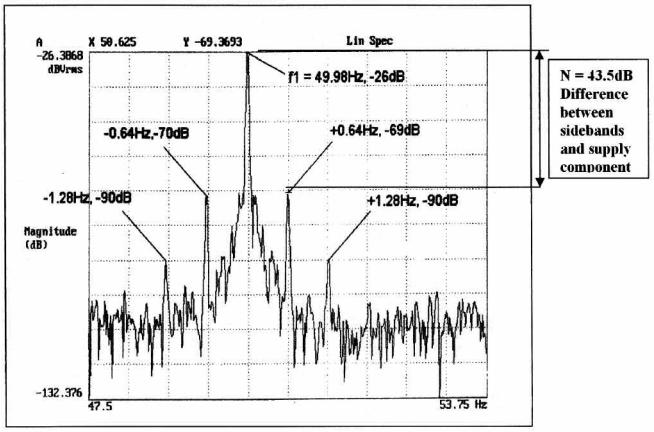

Figure 14. Current Spectrum (or Signature)—Strategic LP Compressor Motor.

Interpretation

There are sidebands at ±0.64 Hz around the supply frequency (49.98 Hz). These are the twice slip frequency sidebands due to a broken rotor bar problem for this motor when operating at a reduced load (104 A) compared to the full-load current of 120 A. It has been proven via numerous case histories that the dB difference (*N*) between the sidebands and the supply component can be used to estimate the severity of the broken rotor bar problem. The operators had to avoid secondary damage to the stator winding (refer to Figures 7 and 8 for an example), and the crucial questions to be answered were:

- How severe is the problem?
- Can the motor be kept running?
- What are the chances of a broken bar hitting the stator winding?

An estimate of the number of broken bars (broken bar factor) can be obtained from the following equation (Thomson and Rankin, 1987):

$$n = \frac{2R}{\left(10^{\frac{N}{20}} + p\right)} = \frac{2 \times 60}{\left(10^{\frac{43.5}{20}} + 2\right)} = 0.79 \quad (3)$$

where:
n = Estimate of number of broken bars
R = Number of rotor slots
N = Average dB difference between upper and lower sidebands and supply component = (43 + 44)/2 = 43.5 dB
p = Pole-pairs = 2

The broken bar factor = 0.79, but Equation (3) is for full-load operation and this has to be corrected since the MCSA measurement was taken on reduced load. Applying the correction factor for this load and particular motor design (commercially sensitive and cannot be released), then the broken bar factor is: n = 1.15. It was therefore predicted that there was definitely one bar completely broken. There was also a risk of the broken bar lifting out of the slot with consequential mechanical damage to the HV stator winding and failure as was illustrated in another case as shown in Figures 7 and 8.

The motor was regularly monitored to trend any further deterioration. A new rotor was immediately ordered, and a spare one was located in storage. The spare one was refurbished by the manufacturer since it had been in storage for 14 years. The faulty rotor was removed and the replacement one installed with a total planned outage of five days on the offshore oil and gas production platform. Note that special scaffolding had to be constructed, etc., for removal of the rotor within the modular construction. Inspection of the faulty rotor, as shown in Figure 15, proved that the diagnosis was correct and that there was one completely broken rotor bar. In fact there was only 40 thou/40 mils/1 mm of laminated steel left at the top of the slot, and note the damage to the rotor core. There was a very high risk of the broken bar lifting out of the slot with consequential mechanical damage to the HV stator winding and a very lengthy outage as previously discussed.

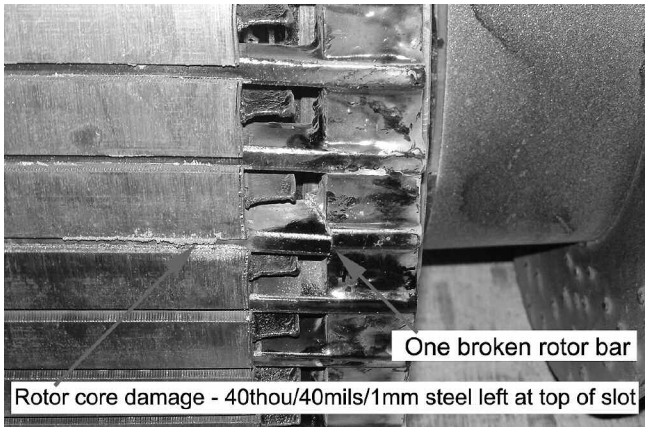

Figure 15. Faulty Rotor Winding Diagnosed via MCSA—Prevented Secondary Damage to HV Stator Winding.

MCSA Airgap Eccentricity Case History

Definition of Airgap Eccentricity—Static and Dynamic

Airgap eccentricity consists of two types, which exist simultaneously in a real SCIM due to manufacturing tolerances/installation procedures (in large motors). First there is static eccentricity, where the position of minimum radial airgap length is fixed in space. It can be caused by stator core ovality or incorrect positioning of the rotor or stator. There is always an inherent level due also to manufacturing tolerances caused by the compound buildup of parts that have their own tolerances. Second there is dynamic eccentricity, where the minimum airgap revolves with the rotor and is a function of space and time. This can be caused by a nonconcentric outer rotor diameter, thermal bowing of the rotor, or bearing wear and movement. The airgap eccentricity specified by a manufacturer is the radial airgap eccentricity (static plus dynamic) and is normally given as a percentage (*e%*) of the nominal radial airgap length (*g*). An illustration of airgap eccentricity is shown in Figure 16.

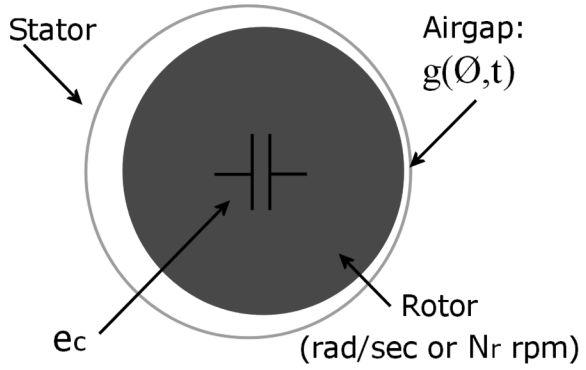

Figure 16. Illustration of Airgap Eccentricity.

Terminology for Defining Airgap Eccentricity

The terminology for defining airgap eccentricity is as follows:

g = Nominal radial airgap length (manufacturer's specification in inches or mm)
$g_{(Ø,t)}$ = Radial length of airgap around periphery in inches or mm
e_c = Absolute value of airgap eccentricity, normally in thousands of an inch (mils) or in mm
e% = Overall percentage airgap eccentricity = e_c/g
w = Rotational speed of rotor, rad/sec
Ø = Angular distance around airgap, degrees

For completeness, the airgap length of both static (e_s) and dynamic eccentricity (e_d) can be expressed as:

$$g_{(\phi,t)} = g\left(1 - e_s \cos\phi - e_d \cos(\omega t - \phi)\right) \tag{4}$$

A Practical Illustration

A practical illustration follows. Recall: 1 thou = 0.001 inches (1 mil) = 0.0254 mm. Let the nominal radial airgap length g = 50 thou (50 mil) or 1.27 mm. An airgap eccentricity of (*e*%) 10 percent would give: $g_{(Ø,t)}$ = 50 thou ± 5 thou (50 mils ± 5 mils) or 1.27 mm ± 0.127 mm. A minimum and maximum airgap length of 45 and 55 thou (45 mil and 55 mil) or 1.143 and 1.397 mm, respectively.

Typical Examples of Industrial SCIMs

- *Example one*—An eight-pole, 11 kV, 1.45 MW/1944 hp, 103 A, 742 rpm, 50 Hz, three-phase, SCIM has an airgap length specification of 100 thou ± 5 percent or 2.5 mm ± 5 percent, which is 100 thou ± 5 thou or 2.5 mm ± 0.125 mm. This is an actual manufacturer's specification. The total indicated reading (TIR) on a concentricity check on the rotor at manufacture = 2 thou or 0.05 mm. This gives a dynamic eccentricity of 2 percent. The total airgap eccentricity tolerance is 5 percent, thus leaving an allowable static eccentricity of 3 percent.

- *Example two*—A four-pole, 415 V, 11 kW/14.75 hp, SCIM, 50 Hz, 20.5 A, 1440 rpm has an airgap length specification of 15 thou ± 10 percent, or 0.381 mm ± 10 percent, which is 15 thou ± 1.5 thou or 0.381 mm ± 0.0381 mm.

- *Example three*—An 11 kV, 5 MW/6702 hp, two-pole motor would have an airgap in the order 200 thou ± 5 to 10 percent or 5 mm ± 5 to 10 percent.

Causes and Effects of Airgap Eccentricity Problems in Induction Motors

Static eccentricity causes a steady force called unbalanced magnetic pull (UMP) on the rotor in one direction that tries to pull the rotor even further from the stator bore center in the direction of the minimum airgap as shown in Figure 17. The resistance to this further reduction in the airgap is primarily controlled by the mechanical stiffness of the rotor. Flexible rotors are therefore more prone to rotor to stator rubs due to high UMP.

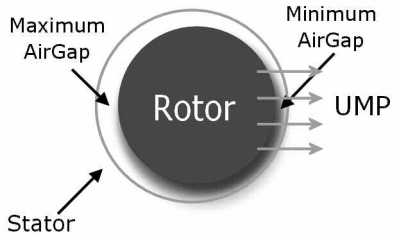

Figure 17. Illustration of UMP.

Dynamic eccentricity causes a force (rotating UMP) that acts on the rotor, but it rotates at the rotor speed (i.e., a rotating force wave). If the levels of airgap eccentricity are not kept within specified limits (e.g., typically a maximum of 10 percent in three-phase induction motors), then both types of eccentricity can cause excessive stressing of the motor and can increase bearing wear. The radial magnetic force waves produced by eccentricity also act on the stator core assembly and rotor cage, and thus subject the stator and rotor windings to unnecessary and potentially harmful vibration. High UMP due to severe airgap eccentricity can ultimately lead to a rotor to stator rub with consequential damage to the core and stator windings or the rotor cage. A rotor to stator rub can cause insulation failure of the stator winding or the breaking of rotor cage bars or end rings and, hence, a costly repair in a large, HV, induction motor. Acoustic noise levels can substantially increase due to high levels of airgap eccentricity.

Comments on the Severity of Airgap Eccentricity

Manufacturers make every effort to keep airgap eccentricity to a minimum due to the damaging forces and effects that abnormal levels of eccentricity can produce. Some manufacturers and users specify a maximum permissible level of 5 percent, whereas in other cases, a maximum level of 10 percent is allowed by the user. There is no doubt that when the airgap eccentricity starts to increase above 25 to 30 percent of the nominal airgap length, then there will be substantial forces and potentially serious secondary effects as specified above (Bonnet and Soukup, 1992). In large three-phase induction motors, a level of 25 to 30 percent airgap eccentricity can be considered to be severe. The level of eccentricity at which a stator to rotor rub will occur is a function of a number of factors such as mechanical stiffness of the shaft, pole number, flux density levels, and starting cycle when the ampere turns are the greatest, etc.

Diagnosis of an Airgap Eccentricity Problem via MCSA and Case History

The MCSA monitoring strategy is to identify the characteristic current signature pattern that is indicative of abnormal levels of airgap eccentricity and to then trend that signature. The signature pattern given by equation (5) can be used to identify the current signature pattern (Cameron, et al., 1986; and Sobczyk and Weinreb, 1988):

$$f_{ec} = f_1\left\{\left(R \pm n_d\right)\left(\frac{1-s}{p}\right) \pm n_{\omega s}\right\} \tag{5}$$

where:
f_{ec} = Frequency components that are a function of airgap eccentricity (Hz)
f_1 = Supply frequency (Hz)
R = Number of rotor slots
n_d = ±1
n_{ws} = 1, 3, 5, 7
s = Slip
p = Pole-pairs

With n_d = 0 in Equation (5), this gives the classical rotor slot passing frequency components—a series of components spaced at twice the supply frequency (2f1) apart. With n_d = ±1 in Equation (5), this gives additional components that were initially (1985/1986) thought to be only a function of dynamic airgap eccentricity (Cameron, et al., 1986). However, extensive experimental tests subsequently proved that, as static eccentricity increased, the components that were theoretically supposed to be only a function of dynamic eccentricity also increased in magnitude (Thomson and Barbour, 1998). Finite element studies and further laboratory tests and industrial case histories have proved that these components are in fact a function of the combination of static and dynamic airgap eccentricity, namely the overall airgap eccentricity (Thomson and Barbour, 1998). The signature pattern of specific rotor slot passing frequencies and the two com-

ponents from Equation (5) with $n_d = \pm 1$ (actually spaced at $\pm f_r$—rotational speed frequency around the rotor slotting components) can be used to identify abnormal levels of airgap eccentricity as will be demonstrated in the case history.

Airgap Eccentricity Case History—
Large Pump Drives, Oil Storage Site

Motor nameplate data: three-phase, 11 kV, 1.45 MW/1944 hp, 103 A, 742 rpm, 50 Hz, star-connected, no parallel paths in the stator winding. The rotor slots, R = 62. Four motor-pump drives are used to pump oil from an oil tank farm into large tankers in a nearby deep water estuary. One of the motors had developed a bearing vibration and temperature problem and would only run for 45 minutes since it tripped out on a high bearing temperature of 180°F (85°C). The fundamental cause of the problem could not be determined via vibration analysis. MCSA was applied to determine whether there was an airgap eccentricity problem. Figure 18 shows a portion of the current spectrum (from the faulty motor) with one of the rotor slot passing frequency components (S_{e1}) and the components (d_{e1}, d_{e2}) corresponding to $n_d = \pm 1$ from Equation (5). The signature pattern is characteristic of a motor with an abnormal level of airgap eccentricity. The d_{e1} and d_{e2} components are the same magnitude, namely, 15 dB down on the rotor slot passing frequency S_{e1} for the problem motor. But, in an identical and healthy motor, the d_{e2} component is not present, and the d_{e1} component is 25 dB down on the rotor slot passing frequency component (S_{e1}) as shown in Figure 19 compared to the faulty one shown in Figure 18. The signature pattern in the problem motor is exhibiting the characteristic pattern of a motor with an unacceptable level of airgap eccentricity, namely that both the plus and minus rotational speed frequency components around the rotor slot passing frequency are clearly evident and 15 dB down on S_{e1}. For normal airgap eccentricity levels, the d_{e1} and d_{e2} components should both be greater than 25 to 30 dB down on S_{e1}.

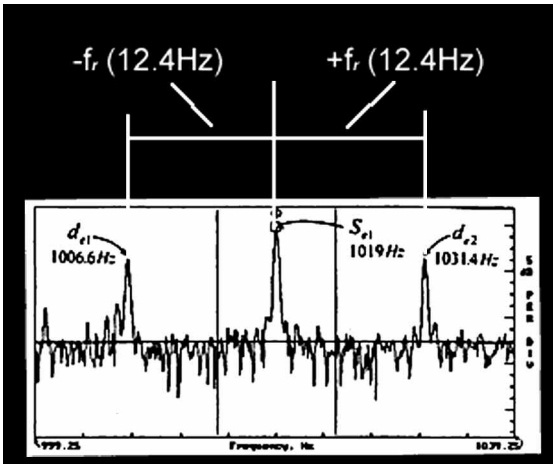

Figure 18. Current Spectrum, Unacceptable Level of Airgap Eccentricity.

This motor had a nominal airgap length of 100 thou or 2.5 mm, and the manufacturer allowed a tolerance of ±5 percent (±5 thou) airgap eccentricity (total of static plus dynamic). The rotor was manufactured to have a total run out of 2 thou or 0.05 mm giving a dynamic eccentricity of just 2 percent. The motor airgaps were checked onsite and were found to be 35 percent and 20 percent at the drive-end and nondrive-end, respectively. It was removed to the manufacturer's workshop, where the rotor runout was checked and was found to be as per the original specification at the time of manufacture. It should be appreciated that although the offline checks gave an airgap eccentricity of 35 percent, this could be higher when the motor was running due to UMP and, of course, could result in

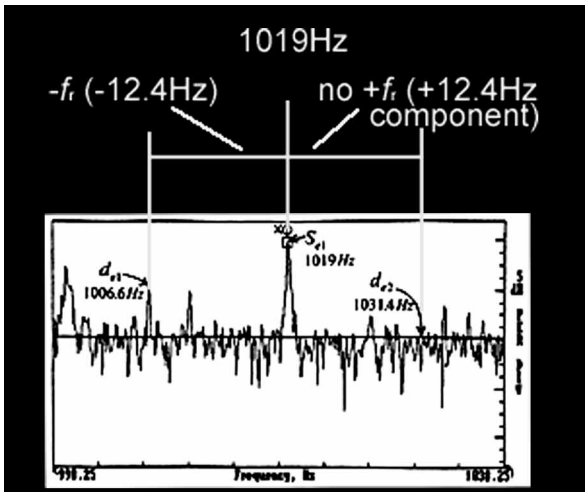

Figure 19. Current Spectrum, Normal Level of Airgap Eccentricity.

a higher dynamic eccentricity, due to any bow in the rotor as a by-product of the high static airgap eccentricity. The problem was primarily high static airgap eccentricity, and the motor was reassembled and installed to ensure the overall airgap eccentricity level was not greater than ±10 percent of the nominal airgap length. The high bearing temperature and vibration problem was eliminated, which proved that MCSA had identified the root cause of the initial problem.

MCSA Shorted Turns in Low Voltage Stator Case History

Introduction to Low Voltage Stator Winding Faults

In fixed frequency, low voltage, main's fed induction motors, it is generally accepted that there is normally no prewarning of insulation degradation. It is normally the case that insulation degradation in main's fed, low voltage stator windings cannot be initially diagnosed via online measurements, and the first indication of a problem will be that a fault actually develops. It should be emphasized that there is a clear distinction between partial discharge (PD) monitoring to diagnose insulation degradation prior to a fault in HV machines (Kurtz, et al., 1984) and MCSA to detect shorted turns in a LV induction motor (Thomson and McCrae, 1989; and Thomson, 2001). With respect to low voltage stator windings, the faults can be classified as follows:

1. *Turn-to-turn shorts within a coil*—Motor will continue to operate but for how long?

2. *Short between coils of the same phase*—Motor can continue to operate but for how long?

3. *Phase-to-phase short*—Motor fails and protection equipment disconnects the supply.

4. *Phase-to-earth short*—Motor fails and protection equipment disconnects the supply.

5. *Open circuit in one phase (single-phasing)*—Motor may continue to operate depending on the load condition (e.g., at no-load or light load running) and protection equipment.

Prewarning of motor failure such as in 3 and 4 above can only be achieved if shorted turns within a coil (e.g., one or two shorted turns) are initially diagnosed via online diagnostic techniques. This requires continuous online monitoring to diagnose the faults stated in 1 and 2 above for low voltage induction motors. There is also the question of how long it takes for shorted turns within a coil to develop into a phase-to-phase or phase-to-earth fault and motor failure in low voltage machines. There is not a simple, qualitative answer to that question, since it will be a function of many variables and will in fact be unique to each motor. However, the

general opinion of manufacturers and users is that there can be a longer lead time between the inception of shorted turns up to failure in an LV motor in comparison to an HV motor. Some operators and manufacturers have previously considered that it is not worth diagnosing shorted turns in stator windings of LV induction motors since the lead time to a failure is too short to merit an online diagnostic system.

The concept that the motor has already developed a fault and will need to be repaired has prevailed; hence, if it is a low voltage induction motor then often the approach is to let it run to failure. However, in modern production processes any lead-time can be extremely advantageous since unexpected failure of a strategic, low voltage, induction motor drive can be very costly, and, in some industries, it can also be a serious safety hazard. If shorted turns (e.g., one or two turns) in a stator coil can be diagnosed, a pre-planned shutdown can be arranged for the motor to be replaced by a healthy one, and the faulty one is sent for repair. Excellent examples of typical failures in random wound, low voltage induction motors are shown by Bonnet and Soukup (1992).

Predictor Equation for Diagnosis of Shorted Turns via MCSA

The objective is to identify current components in the stator winding that are only a function of shorted turns and are not due to any other problem or mechanical drive characteristic. There has been a range of papers published on the analysis of airgap and axial flux signals to detect shorted turns, and the detailed mathematics can be found in Tavner and Penman (1987) and in Thomson (2001). Previous studies have proved that the following equation gives the components in the airgap flux waveform that are a function of shorted turns:

$$f_{st} = f_1\left\{\frac{n}{p}(1-s) \pm k\right\} \tag{6}$$

where:
f_{st} = Components that are a function of shorted turns
f_1 = Supply frequency
n = 1, 2, 3, …
k = 1, 3, 5, …
p = Pole-pairs
s = Slip

The diagnosis of shorted turns via MCSA is based on detecting the frequency components given by Equation (6) in that these rotating flux waves can induce corresponding current components in the stator winding. Full details of the theory and application of MCSA to diagnose shorted turns in low voltage stator windings can be found in Thomson (2001). Motors with different winding designs, pole numbers, and power ratings were tested until failure under different load conditions, and that was the first time results had been presented from motors just prior to actual failure from shorted turns.

Case History on the Diagnosis of Shorted Turns in a LV Stator Winding via MCSA

Results from an 11 kW, 415/420 V, 20.5 A, 1440 rpm, 50 Hz, SCIM, delta connected motor are now reported. The stator winding was a three tier concentric winding with random wound coils in 36 slots. There were two coils per group, four groups per phase, and each group had coils of 15 and 30 turns, respectively, giving 180 turns per phase. Figures 20 and 21 show the current spectra with no fault and the case with actual shorted turns. The components that are clearly indicative of shorted turns under no-load are 125 Hz and 175 Hz, as per Equation (6), with k = 1, n = 3, and k = 1, n = 5. Note that the components at 25 Hz and 75 Hz are present under normal operation (the ± rotational speed frequency components) and cannot be used as indicators of shorted turns even although they are predicted from Equation (6). There are no current components at 125 and 175 Hz (no-load slip is approximately zero for Equation (6)) with no stator fault, but they are very evident at 56.6 and 42.3 dB, respectively, in the case with direct shorted turns. Thomson (2001) has shown that these components could also be detected at 27.7 and 23.6 dB, respectively, with one shorted turn via a current limiting resistor to avoid initial burnout.

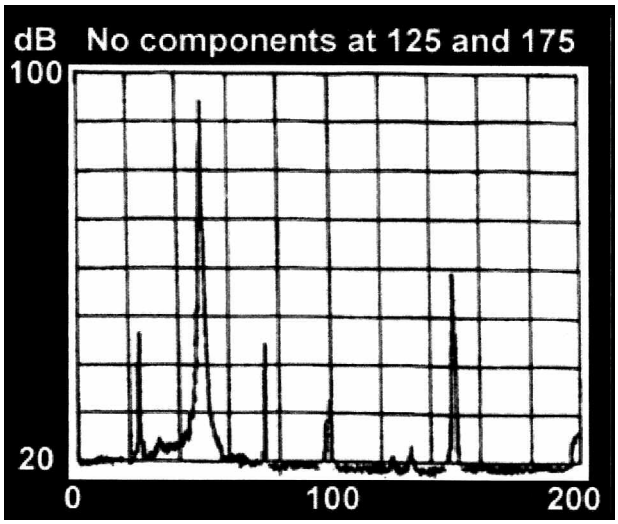

Figure 20. Current Spectrum—Healthy Stator.

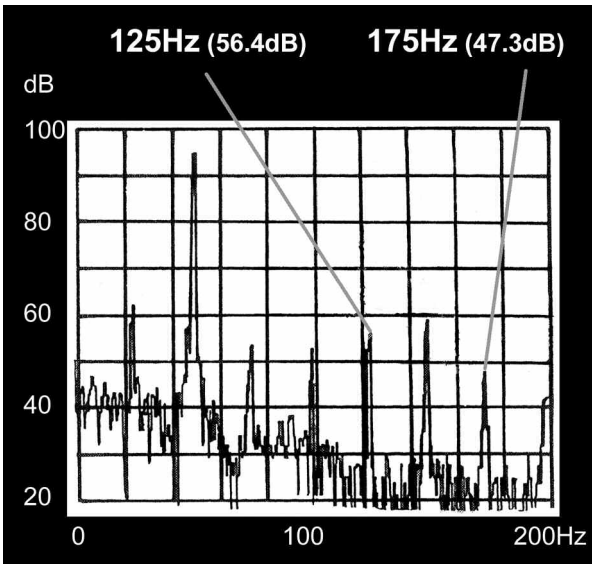

Figure 21. Current Spectrum—Shorted Turns.

Figure 22 shows the faulty stator winding. This demonstrates that these two components are good indicators for detecting shorted turns in four-pole SCIMs with random wound, concentric coils. Note that these components will change in frequency as a function of load and speed, as reported by Thomson (2001). Note that a continuous MCSA system must be used to detect shorted turns.

CONCLUSIONS

Industrial case histories have clearly demonstrated that MCSA is a powerful online monitoring technique for assessing the operational condition of three-phase induction motors. The avoidance of catastrophic failures can be achieved via MCSA and other major benefits include the prevention of lost downtime, avoidance of

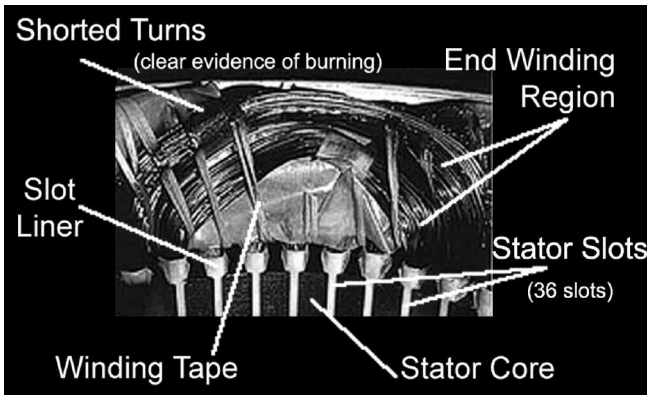

Figure 22. Faulty Stator Winding Diagnosed via MCSA.

major motor repair, or replacement costs. Of course the bottom line is the prevention of lost income being the key driver for using MCSA to assess the operational condition of strategic induction motor drives. The importance of applying induction motor fundamentals, understanding signal processing concepts, paying particular attention to detail when taking MCSA measurements to ensure reliable data, appreciating the operational conditions of the motor, and, of course, correct interpretation of the data have been illustrated in this paper. It is emphasized that knowledge on the design and operation of induction motors are crucial ingredients for correct data interpretation and a reliable diagnosis of the operational condition of the motor. Additional case histories will also be presented and discussed at the tutorial presentation.

APPENDIX A— FUNDAMENTALS ON TWICE SLIP FREQUENCY SIDEBANDS DUE TO BROKEN ROTOR BARS

- The general equation that relates the supply frequency (f_1) of the voltage supply to a three-phase stator winding, the synchronous speed (N_s) of the rotating magnetic field produced by the stator winding, and (p) the pole-pairs of the winding is given by:

$$f_1 = N_s \times p \tag{A-1}$$

- Under perfectly balanced conditions then only a forward rotating field is produced, which rotates at synchronous speed.

- The rotor rotates at N_r, and Figure A-1 illustrates that the rotor always rotates at a speed less than the synchronous speed. A measure of the slipping back of the rotor is termed the slip, defined as:

$$Slip\ s = \left(N_s - N_r\right) / N_s \tag{A-2}$$

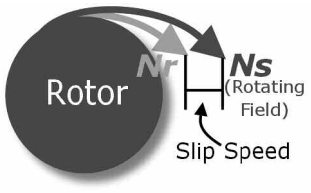

Figure A-1. Illustration of Slip Speed.

- This is in fact a per unit term and is often presented as a percentage.

The slip speed = $N_s - N_r$, as illustrated in Figure (A-1), is the actual difference in rpm between the speed of the rotating magnetic field and the actual speed of the rotor, but note that the slip frequency is not the slip speed divided by 60 to convert to Hertz. The term slip frequency in induction motor theory has a specific definition and is as follows:

- The frequency of the rotor currents is given a specific name in induction motor theory, namely, the slip frequency (f_2) and is derived as follows:

$$f_2 = \left(N_s - N_r\right)p = s \times N_s \times p \tag{A-3}$$

$f_2 = sf_1$ = Slip frequency and is purely defining a specific electrical quantity.

- Under normal operation, the rotating magnetic field produced by the currents flowing in the rotor conductors moves faster than the actual rotor speed (N_r), as illustrated in Figure A-2.

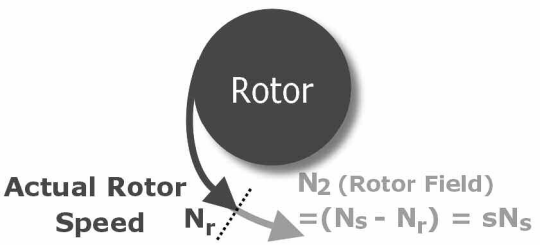

Figure A-2. Illustration of Rotating Field from Rotor Currents Moving Faster than Rotor Speed.

- Now the speed of the rotating magnetic field produced by the current carrying rotor conductors with respect to the stationary stator winding is given by:

$$N_r + N_2 = N_r + N_s - N_r = N_s \tag{A-4}$$

- With respect to a stationary observer on the fixed stator winding, then the speed of the rotating magnetic field from the rotor equals the speed of the stator rotating magnetic field, namely, the synchronous speed, N_s. This is an important result, but initially it can be conceptually difficult to understand. Both fields are locked together to give a steady torque production by the induction motor.

With Broken Rotor Bars

With broken rotor bars there is an additional rotating magnetic field produced. Broken rotor bars produce a backward rotating field at slip speed (-ve direction ($N_s - N_r$) = sN_s) with respect to the rotor as illustrated in Figure A-3.

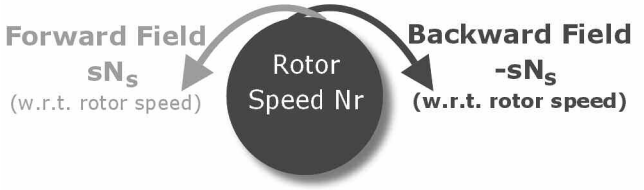

Figure A-3. Illustration of Forward and Backward Rotating Fields from Rotor Currents When a Broken Bar Exists.

What does the Stationary Stator Winding Observe?

- Let N_b = backward rotating magnetic field speed produced by the rotor due to broken bars = $N_r - sN_s$

$$Slip\ s = \left(N_s - N_r\right) / N_s \ and\ N_r = N_s(1-s)$$
$$N_b = N_r - sN_s = N_s(1-s) - sN_s = N_s - 2sN_s \tag{A-5}$$
$$N_b = N_s - 2sN_s$$

- The stationary stator winding now sees a rotating field at:

$$N_b = N_s - 2sN_s \tag{A-6}$$

• Expressed in terms of frequency, speed of rotating magnetic field, and number of pole pairs this gives:

$$\begin{aligned} f_b &= \left(N_s - 2sN_s\right)p \\ f_b &= \left(\left(f_1 / p\right) - 2s\left(f_1 / p\right)\right)p \\ f_b &= \left(f_1 - 2sf_1\right) \end{aligned} \tag{A-7}$$

• Equation (A-7) means that a rotating magnetic field at that frequency cuts the stator windings and induces a current at that frequency (f_b).

• This in fact means that (f_b) is a twice slip frequency component spaced $2sf_1$ down from f_1.

• Speed and torque oscillations occur at $2sf_1$, and this induces an upper sideband at $2sf_1$ above f_1.

• *Classical twice slip frequency sidebands therefore occur at* $\pm 2sf_1$ *around the supply frequency.*

REFERENCES

Alger, P. L., 1965, *Induction Machines*, New York, New York: Gordon and Breach.

Bonnet, A. H. and Soukup, G. C., 1992, "Cause and Analysis of Stator and Rotor Failures in Three-Phase Squirrel-Cage Induction Motors," *IEEE Transactions on Industry Applications*, 28, (4), pp. 921-937.

Cameron, J. R., Thomson, W. T., and Dow, A. B., May 1986, "Vibration and Current Monitoring for Detecting Airgap Eccentricity in Large Induction Motors," *IEE Proceedings*, *133*, Part B, (3).

Finley, W. R. and Hodowanec, M. M., Nov/Dec 2001, "Selection of Copper Versus Aluminum Rotors for Induction Motors," *IEEE Transactions on Industry Applications*, *37*, (6), pp. 1563-1573.

Hargis, C., Gaydon, B. G., and Kamish, K., 1982, "The Detection of Rotor Defects in Induction Motors," *Proceedings of IEE EMDA Conference*, London, England, pp. 216-220.

Kliman, G. B. and Stein, J., 1990, "Induction Motor Fault Detection via Passive Current Monitoring," *Proceedings of International Conference (ICEM'90)*, Massachusetts Institute of Technology, Boston, Massachusetts, pp. 13-17.

Kurtz, M., Lyles, J. F., and Stone, G. C., 1984, "Application of Partial Discharge Testing to Hydrogenerator Maintenance," *IEEE Transactions*, PAS, *PAS-103*, pp. 2146-2157.

Sobczyk, T. J. and Weinreb, K., 1988, "Synthesis of Mathematical Models of Induction Machines with Non-Uniform Airgap," *Proceedings of ICEM'88*, Pisa, Italy, *1*, pp. 287-2912.

Tavner, P. and Penman, J., 1987, *Condition Monitoring of Electrical Machines*, Research Studies Ltd., London, England: John Wiley & Sons.

Thomson, W. T., 1984, "Diagnosing Faults in Induction Motors—Engineering Ideas," *Electrical Review*, *215*, (17).

Thomson, W. T., 1999, "A Review of On-Line Condition Monitoring Techniques for Three-Phase Squirrel-Cage Induction Motors—Past, Present, and Future," *IEEE Symposium on Diagnostics for Electrical Machines, Power Electronics and Drives*, Gijon, Spain, pp. 3-18 (opening keynote address).

Thomson, W. T., 2001, "On-Line MCSA to Diagnose Shorted Turns in Low Voltage Stator Windings of 3-Phase Induction Motors Prior to Failure," *Proceedings of IEEE Conference on Electrical Machines and Drives (IEMDC)*, Massachusetts Institute of Technology, Boston, Massachusetts.

Thomson, W. T. and Barbour, A., December 1998, "On-line Current Monitoring and Application of a Finite Element Method to Predict the Level of Airgap Eccentricity in 3-Phase Induction Motors," *IEEE Transactions on Energy Conversion*, *13*, (4), 1998, pp. 347-357 (includes discussion and closure).

Thomson, W. T. and McRae, C., 1989, "On-Line Current Monitoring to Detect Inter-Turn Winding Faults in Induction Motors," *24th Universities Power Engineering Conference*, Queen's University, Belfast, Ireland.

Thomson, W. T. and Orpin, P., 2002, "Current and Vibration Monitoring for Fault Diagnosis and Root Cause Analysis of Induction Motor Drives," *Proceedings of Thirty-First Turbomachinery Symposium*, Turbomachinery Laboratory, Texas A&M University, College Station, Texas, pp. 61-67.

Thomson, W. T. and Rankin, D., 1987, "Case Histories of Rotor Winding Fault Diagnosis in Induction Motors," *Proceedings Second International Conference on Condition Monitoring*, University College of Swansea, Wales, United Kingdom.

Thomson, W. T., Rankin, D., and Dorrell, D. G., 1999, "On-line Current Monitoring to Diagnose Airgap Eccentricity—An Industrial Case History of Large HV, 3-Phase Induction Motors," *IEEE Transactions on Energy Conversion*.

Williamson, S. and Smith, A. C., May 1982, "Steady State Analysis of 3-Phase Cage Motors with Rotor-bar and End-ring Faults," *Proceedings of IEE*, *129*, Part B, (3), pp. 93-100.

Yang, S. J., 1981, "Low Noise Electric Motors," Monographs in Electrical and Electronic Engineering, IEE, Savoy Place, London, England.